TRAVELING BREATHERS AND SOLITARY WAVES IN STRONGLY NONLINEAR LATTICES

GUILLAUME JAMES[1,2]

Abstract. We study the existence of traveling breathers and solitary waves in the discrete p-Schrödinger (DpS) equation. This model consists of a one-dimensional discrete nonlinear Schrödinger equation with strongly nonlinear inter-site coupling (a discrete p-Laplacian). The DpS equation describes the slow modulation in time of small amplitude oscillations in different types of nonlinear lattices, where linear oscillators are coupled to nearest-neighbors by strong nonlinearities. Such systems include granular chains made of discrete elements interacting through a Hertzian potential ($p = 5/2$ for contacting spheres), with additional local potentials or resonators inducing local oscillations. We formally derive three amplitude PDE from the DpS equation when the exponent of nonlinearity is close to (and above) unity, i.e. for p lying slightly above 2. Each model admits localized solutions approximating traveling breather solutions of the DpS equation. One model is the logarithmic nonlinear Schrödinger (NLS) equation which admits Gaussian solutions, and the other are fully nonlinear degenerate NLS equations with compacton solutions. We compare these analytical approximations to traveling breather solutions computed numerically by an iterative method, and check the convergence of the approximations when $p \to 2^+$. An extensive numerical exploration of traveling breather profiles for $p = 5/2$ suggests that these solutions are generally superposed on small amplitude nonvanishing oscillatory tails, except for particular parameter values where they become close to strictly localized solitary waves. In a vibroimpact limit where the parameter p becomes large, we compute an analytical approximation of solitary wave solutions of the DpS equation.

1. Introduction

Energy localization in discrete media occurs in many contexts, such as the propagation of stress waves in granular media [49, 51] (or voltage pulses in nonlinear transmission lines [1]), the excitation of nonlinear oscillations in crystals by atom bombardment [13, 14], and the nonlinear localization of vibrations in macromolecules [53]. In this framework, nonlinear Hamiltonian lattices consisting of one-dimensional chains of coupled oscillators (spatially homogeneous or periodic) have been widely analyzed. Relevant phenomena include the propagation of solitary waves [23] (spatially localized traveling waves), as well as the trapping of vibrational evergy in the form of discrete breathers, i.e. spatially localized oscillations [45] (see [22, 20, 10, 35] for more references). In addition, the analysis of traveling breathers constitutes a notoriously difficult problem, see e.g. [30, 22, 20] for reviews. Modulation theory based on the Korteweg–de Vries (KdV) equation [4, 36, 58] and the nonlinear Schrödinger (NLS) equation [26, 57] constitutes a classical approach to approximate small amplitude solitary waves and static or traveling breathers over long time scales.

In this paper, we consider more specifically *strongly nonlinear* lattices for which all oscillators become uncoupled in the linearized equations, so that energy cannot propagate through purely linear effects. Another direct consequence of strong nonlinearity is that the usual KdV and NLS asymptotics describing the balance between linear dispersion and nonlinearity do not apply. One application of strongly nonlinear lattices comes from the design of granular crystals [54, 64, 60, 49] (or other kinds of highly nonlinear acoustic metamaterials) for the passive

Date: December 11, 2018.

control of acoustic waves, including impact mitigation and redirection, acoustic lensing and filtering. In granular crystals, contact interactions between discrete elements are governed by the (generalized) Hertzian potential

$$V(x) = \frac{1}{p}\,(-x)_+^p, \tag{1}$$

where $p > 2$, $(x)_+ = \max(x, 0)$ and nonlinear stiffness has been normalized to unity. This potential describes the contact force $\propto (-x)_+^\alpha$ (with $\alpha = p - 1$) between two initially tangent elastic bodies (in the absence of precompression) after a small relative displacement x. The most classical case is obtained for $p = 5/2$ ($\alpha = 3/2$) and corresponds to contact between spheres, or more generally two smooth non-conforming surfaces.

An example of granular metamaterial is given by the so-called locally resonant granular chain. Such metamaterials have been experimentally tested in the form of chains of spherical beads with internal linear resonators (mass-in-mass chain) [8], granular chains with external ring resonators attached to the beads (mass-with-mass chain) [24] (see also [39]) and woodpile phononic crystals consisting of vertically stacked slender cylindrical rods [41, 42]. Under certain conditions, each of these systems can be described by a chain of particles coupled to nearest-neighbors by a Hertzian potential, with a secondary mass attached to each element by a linear spring. The dynamical equations take the form

$$\begin{aligned} \ddot{u}_n + u_n &= V'(u_{n+1} - u_n) - V'(u_n - u_{n-1}) + v_n \\ \ddot{v}_n &= \omega^2\,(u_n - v_n), \end{aligned} \tag{2}$$

where $u_n(t)$ and $v_n(t)$ denote the (dimensionless) displacements of the nth primary and secondary masses, respectively. The frequency ω corresponds to the (rescaled) natural frequency of the internal or external resonators [8, 24] or the primary bending vibration mode of the cylindrical rods in the woodpile setup [41]. Alternatively, $\rho = 1/\omega^2$ can be interpreted as the rescaled mass of the local resonators.

In the limit $\rho \to 0$, one obtains $u_n = v_n$ and the model (2) reduces to the one for a regular (non-resonant) homogeneous granular chain, which is known to support compression solitary waves [49, 2, 23, 46, 65, 28]. The width of these solitary waves is independent of their amplitude and their spatial decay is doubly-exponential [15, 65]. In the opposite limit with $\omega \to 0$ and zero initial conditions for $v_n(t)$ the system approaches a model of Newton's cradle (see figure 1, left panel), a granular chain with quadratic onsite potential, which is governed by

$$\ddot{u}_n + u_n = V'(u_{n+1} - u_n) - V'(u_n - u_{n-1}). \tag{3}$$

Both static and traveling breather solutions have been found numerically in system (3) [31, 63, 32]. It is therefore not surprising that for finite values of ω, the model (2) admits a rich variety of localized solutions, namely solitary waves [38], weakly nonlocal solitary waves or nanoptera [42, 71, 69, 38], long-lived static breathers [44] and traveling breathers (see figure 1, right panel).

The analytical study of static and traveling breathers in systems (2) and (3) is quite delicate. Due to the lack of smoothness (for $p = 5/2$) and strongly nonlinear character of the Hertzian interaction potential, classical approaches based on spatial center manifold reduction [33] or NLS reduction [26, 57] do not apply. In addition it has been proved it [44] that exact time-periodic breathers do not exist in system (2) (i.e. without precompression of the chain), despite the fact that similar excitations can persist over long (but finite) times.

An interesting insight into the dynamics of systems (2) and (3) can be obtained through the analysis of a spatially discrete modulation equation, namely the discrete p-Schrödinger (DpS)

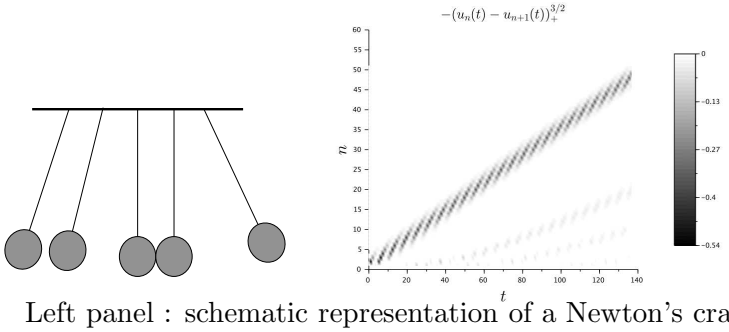

FIGURE 1. Left panel : schematic representation of a Newton's cradle. Right plot : space-time evolution of the contact forces $V'(u_{n+1}-u_n)$ (gray levels) for system (1)-(2) with $p = 2.5$ and $\rho = 3$. We simulate a chain of 52 particles with fixed-end boundary conditions, i.e. $u_0 = u_{51} = 0$. A unit initial velocity is given to first the primary mass (i.e. $\dot{u}_1(0) = 1$), while all the other elements are initially at rest. This excitation generates a localized propagating wave taking the form of a traveling breather (its internal oscillations are clearly visible through an alternance of black and gray strips).

equation introduced in [31]. This model reads

$$i\frac{d}{dt}a_n = (\Delta_p a)_n, \quad n \in \mathbb{Z}, \tag{4}$$

where $a(t) = (a_n(t))_{n\in\mathbb{Z}}$ denotes a time-dependent complex sequence and

$$(\Delta_p a)_n = (a_{n+1}-a_n)\,|a_{n+1}-a_n|^{p-2} - (a_n - a_{n-1})\,|a_n - a_{n-1}|^{p-2}$$

the discrete p-Laplacian with $p > 2$. This model is reminiscent of the discrete nonlinear Schrödinger (DNLS) equation studied in detail in a number of different contexts, including nonlinear optics and atomic physics [37]. However, the DpS equation is fundamentally different in that it contains a fully nonlinear inter-site coupling term and shares some structural similarities with the Fermi-Pasta-Ulam (FPU) model with homogeneous potential [43, 19, 18, 61].

The DpS equation describes how small amplitude oscillations of the Newton's cradle (3) are slowly modulated in time [31, 63, 32, 6], and it achieves the same (for well-prepared initial data) for the locally resonant granular chain (2) when ω is small (or equivalently when the attached mass ρ is large) [44]. To be more precise, let ϵ denote a small parameter and $\omega = \mathcal{O}(\epsilon^{\alpha-1})$ in (1)-(2) ($\alpha > 1$). Consider a solution a of (4) and the Ansatz $u_n^{a,\epsilon}(t) = \epsilon\, a_n(\omega_0\, \epsilon^{\alpha-1}\, t)\, e^{i\, t} + \text{c.c.}$, where ω_0 is an appropriate renormalization constant depending solely of α [44] and c.c. stands for complex conjugate. In that case (see Theorem 3.1 in [44]), for all ϵ small enough, if $(u_n, \dot{u}_n)$ is $\mathcal{O}(\epsilon^\alpha)$-close to $(u_n^{a,\epsilon}, \dot{u}_n^{a,\epsilon})$ at $t = 0$ and $(v_n, \epsilon^{1-\alpha}\dot{v}_n) = \mathcal{O}(\epsilon^\alpha)$ at $t = 0$, then the same bounds hold true over long times $\mathcal{O}(\epsilon^{1-\alpha})$. In particular, all localized solutions of the DpS equation provide localized solutions of (1)-(2) persisting over long times.

The existence of time-periodic breather solutions with super-exponential localization has been proved in [34] for the DpS equation (4), thereby implying the existence of long-lived static breathers in systems (3) [6] and (2) [44]. The existence of solitary waves and traveling breathers is still an open question for the DpS equation, despite traveling breathers have been found in dynamical simulations [31, 32, 34, 63]. Such solutions correspond to long-lived traveling breather solutions of the Newton's cradle (3) and the locally resonant granular chain (2).

In the present paper, we extend to the setting of traveling breathers an idea used in [34] to approximate time-periodic breathers in the DpS equation. In this work, it was shown numerically that breather envelope converges towards a Gaussian when the nonlinearity exponent is

close to unity, i.e. $p \to 2^+$. This asymptotic behavior was explained by relating the stationary DpS equation to a stationary logarithmic Schrödinger equation [5], the latter having explicit Gaussian solutions. It is interesting to notice that the case when p is relatively close to 2 is not merely a mathematical game. Indeed granular chains involving different orders of nonlinearity have recently attracted much attention, see [59, 67] and references therein. In particular, experimental and numerical studies on solitary wave propagation have been performed with chains of hollow spherical particles of different width [50] and chains of cylinders [40], leading to different values α in the range $1.15 \leq \alpha \leq 1.5$ (see also [66] for other systems with α close to unity).

The traveling breathers considered in the DpS equation (4) take the specific form $a_n(t) = y(n - v\,t)\,e^{-i\,\theta\,n}$, where y is spatially localized, v denotes the breather velocity and $-\theta$ corresponds to the breather phase shift after it propagates from one site to the next (hence $\theta = 0$ corresponds to a solitary wave). Using a multiple-scale analysis, we formally derive in section 2 three different PDE describing the slow modulation of periodic traveling waves for $p \approx 2^+$. In section 3, we use these modulation equations to derive approximate traveling breather solutions and analyze their qualitative properties. The first amplitude equation is a (time-dependent) logarithmic Schrödinger equation having Gaussian localized solutions [5] (see [12, 56, 35] for related works on the logarithmic KdV equation). The two additional models correspond to fully nonlinear degenerate NLS equations with compacton solutions (an equation of the same type was derived in [32] in the stationary case and for $p = 5/2$). In section 44.2, we compare the above analytical approximations to traveling breather solutions computed numerically by the Gauss-Newton method. We observe convergence when $p \to 2^+$ and a rather good accuracy for $p = 5/2$.

Further properties of traveling breathers are discussed, in particular the occurrence of small amplitude nonvanishing oscillatory tails consisting of resonant traveling waves, for generic parameter values (sections 33.4 and 4). In addition, we observe a vanishing of the tail for particular parameter values (e.g. specific velocities of a traveling breather having unit energy) where numerical solutions become close to strictly localized solitary waves (section 44.3). We also obtain in section 33.3 an analytical approximation of solitary waves of system (4) when p is large, which corresponds to a "vibroimpact" limit in the Hertz potential (1) (see [25] for related models). Lastly, some open analytical problems are discussed in section 5.

2. Multiscale analysis for $p \to 2^+$

Before examining the limit $p \to 2^+$ of (4), let us consider the case $p = 2$

$$(\,i\frac{d}{dt} - \Delta\,)a = 0, \tag{5}$$

where $\Delta = \Delta_2$ is the usual discrete linear Laplacian. Equation (5) sustains linear waves $a_n(t) = A\,e^{i\,(\Omega\,t - q\,n)}$, where q denotes the wavenumber, $A \in \mathbb{C}$ the wave amplitude, and the frequency Ω is given by the dispersion relation $\Omega(q) = 4\sin^2(q/2)$. In addition, there exist solutions of (5) consisting of modulated waves

$$a_n(t) = e^{i\,(\Omega\,t - q\,n)}\,A_\epsilon(\xi, \tau) \tag{6}$$

where $\epsilon > 0$ is a small scaling parameter, $\tau = \epsilon^2\,t$, $\xi = \epsilon\,(n - c_q\,t)$ and $c_q = \Omega'(q) = 2\,\sin q$ denotes the group velocity [70]. Such solutions can be approximated using solutions of the continuum linear Schrödinger equation [9]. Let us briefly sketch the procedure. Setting

$$A_\epsilon(\xi, \tau) = A(\xi, \tau) + \mathcal{O}(\epsilon), \tag{7}$$

we look for approximate solutions of (5) in the form

$$\tilde{a}_n^{\rm app}(t) = e^{i\,(\Omega\,t - q\,n)}\,A(\xi,\tau), \tag{8}$$

where the envelope function A is assumed sufficiently smooth. After lengthy but straightforward computations, one obtain the residual error

$$E^{\rm lin} := (\,i\frac{d}{dt} - \Delta\,)\tilde{a}^{\rm app} = \epsilon^2\,e^{i\,(\Omega\,t - q\,n)}\,(i\partial_\tau A - \cos q\,\partial_\xi^2 A) + \mathcal{O}(\epsilon^3). \tag{9}$$

To minimize the residual error when $\epsilon \approx 0$, A has to satisfy the linear Schrödinger equation

$$i\partial_\tau A = \cos q\,\partial_\xi^2 A, \tag{10}$$

which yields $E^{\rm lin} = \mathcal{O}(\epsilon^3)$. If $A(\xi,0)$ displays sufficient smoothness and fast decay at infinity, there exists a modulated wave (6) solution of (5) which satisfies (7) uniformly in $(\xi,\tau) \in \mathbb{R}\times[0,T]$ (this property can be readily seen on the representation of $a_n(t)$ as a Fourier integral [9]). Consequently, the solution (6) remains $\mathcal{O}(\epsilon)$-close to the linear Schrödinger approximation (8) over long times $t = \mathcal{O}(\epsilon^{-2})$.

Extensions of this idea to the weakly-nonlinear setting lead to the NLS equation, see e.g. [26] and references therein. In that case one derives a suitable (small amplitude) Ansatz minimizing the residual error, with a leading order term modulated by the NLS equation, and Gronwall estimates allow to control the resulting approximation over long time scales.

In what follows, we generalize to the nonlinear case the computations performed above for $p = 2$ by considering equation (4) in the limit $p \to 2^+$. In this setting, we do not make any assumption of small amplitude waves. Instead, we consider a family of finite-amplitude periodic traveling waves which are slowly modulated in time (over time scales $t = \mathcal{O}(\epsilon^{-2})$) and space (spatial scale $n = \mathcal{O}(\epsilon^{-1})$). Due to the invariance $n \to -n$ of (5), one can restrict the discussion to wavenumbers $q \in [0,\pi]$ without loss of generality. The results presented below do not apply to solutions of (4) varying slowly in space, so we further assume $q \neq 0$. We investigate solely the different types of amplitude equations resulting from the above limit and do not attempt to provide error bounds.

To determine a suitable scaling relating the small parameters $(p-2)$ and ϵ, we rewrite (4) in the form

$$(\,i\frac{d}{dt} - \Delta_2\,)a = (p-2)\,\delta^+ N_p(\delta^- a), \tag{11}$$

where the forward and backward differences $\delta^\pm$ are defined by

$$(\delta^+ a)_n = a_{n+1} - a_n, \quad (\delta^- a)_n = a_n - a_{n-1}$$

and the nonlinear term of (11) reads

$$N_p(u) = u\,\frac{|u|^{p-2} - 1}{p-2}. \tag{12}$$

Let us denote by $C_{\rm b}^0(\mathbb{R})$ the Banach space of bounded and continuous functions $u : \mathbb{R} \to \mathbb{C}$, endowed with the supremum norm. When $p \to 2^+$, we have in $C_{\rm b}^0(\mathbb{R})$

$$N_p(u) = u\ln|u| + \mathcal{O}(p-2). \tag{13}$$

Since we consider solutions of (4) which are not slowly varying in space, the nonlinear term of (11) is $\mathcal{O}(p-2)$. This leads us to fix $\epsilon^2 = p-2$, so that dispersive and nonlinear effects act on a similar time scale. Moreover, we replace Ansatz (8) by

$$a_n^{\rm app}(t) = \frac{R}{\sqrt{\Omega}}\,\phi_n(t)\,A(\xi,\tau) \tag{14}$$

with $\phi_n(t) = e^{i\,(\Omega\,|R|^{p-2}\,t - q\,n)}$, $\tau = (p-2)\,|R|^{p-2}\,t$, $\xi = \sqrt{p-2}\,(n - c_q\,|R|^{p-2}\,t)$. This Ansatz respects the scaling invariance $a_n(t) \to R\,a_n(|R|^{p-2}\,t)$ of (4).

For $A = 1$, (14) defines exact solutions of (4) corresponding to periodic traveling waves [31]. This is due to the fact that $|(\phi_{n+1} - \phi_n)/\sqrt{\Omega}| = 1$, so

$$(\,i\frac{d}{dt} - \Delta_p\,)\big(\frac{\phi}{\sqrt{\Omega}}\big) = (\,i\frac{d}{dt} - \Delta_2\,)\big(\frac{\phi}{\sqrt{\Omega}}\big) = 0.$$

We now estimate the residual error obtained from (4) and (14) in the case of a general envelope function A (assumed sufficiently smooth). For this purpose we first evaluate $\Delta_p a^{\rm app}$. The expansions performed below are valid when $A(\xi,\tau) \neq 0$ is fixed and $p \to 2^+$.

From the expansions

$$\delta^{\pm} a^{\rm app} = -\,i\,e^{\mp iq/2}\,\sqrt{\Omega}\,a^{\rm app} + \mathcal{O}(\sqrt{p-2}), \tag{15}$$

we obtain

$$|\,\delta^{\pm} a^{\rm app}\,|^{p-2} = |R\,A|^{p-2} + \mathcal{O}((p-2)^{3/2}). \tag{16}$$

Moreover, expanding (15) at higher order, we get

$$\begin{aligned}\delta^{\pm} a^{\rm app} = \frac{R}{\sqrt{\Omega}}\,\phi \quad \times \quad \Big(& -\,i\,e^{\mp iq/2}\,\sqrt{\Omega}\,A + e^{\mp iq}\,\sqrt{p-2}\,\partial_\xi A \\ & \pm \frac{e^{\mp iq}}{2}\,(p-2)\,\partial_\xi^2 A + \mathcal{O}((p-2)^{3/2})\Big). \end{aligned} \tag{17}$$

Since $\Delta_p a^{\rm app} = (\delta^+ a^{\rm app})\,|\delta^+ a^{\rm app}|^{p-2} - (\delta^- a^{\rm app})\,|\delta^- a^{\rm app}|^{p-2}$, combining (16) and (17) yields

$$\Delta_p a^{\rm app} = R\,|R|^{p-2}\phi\,F_p(A), \tag{18}$$

$$F_p(A) = |A|^{p-2}[-\sqrt{\Omega}\,A \,-\, i\frac{c_q}{\sqrt{\Omega}}\sqrt{p-2}\,\partial_\xi A + (p-2)\,\frac{\cos q}{\sqrt{\Omega}}\,\partial_\xi^2 A] + \mathcal{O}((p-2)^{3/2}).$$

Consequently, Ansatz (14) yields the residual error

$$\begin{aligned} E \;&:=\; (\,i\frac{d}{dt} - \Delta_p\,)(a^{\rm app}) && (19)\\ &=\; R|R|^{p-2}\,\phi\,(\,-\sqrt{\Omega}A - \,i\frac{c_q}{\sqrt{\Omega}}\sqrt{p-2}\,\partial_\xi A + \frac{i}{\sqrt{\Omega}}(p-2)\partial_\tau A - F_p(A)\,) \\ &=\; (p-2)\,\frac{R|R|^{p-2}}{\sqrt{\Omega}}\,\phi\,(\,i\partial_\tau A + \Omega\,N_p(A) - \cos q\,(\partial_\xi^2 A)|A|^{p-2} + \mathcal{O}(\sqrt{p-2})\,). && (20)\end{aligned}$$

From this expansion, we deduce different amplitude equations which minimize the residual error when $p \approx 2^+$ and lead to $E = \mathcal{O}((p-2)^{3/2})$. Note that, due to the phase invariance of the nonlinear term N_p of (11), no higher harmonics ϕ^k are generated in (20). As a consequence, it is not necessary to add higher order terms to the Ansatz (14) in order to achieve $E = \mathcal{O}((p-2)^{3/2})$.

The first amplitude equation deduced from (20) is the logarithmic Schrödinger equation (log-NLS)

$$i\partial_\tau A = \cos q\,\partial_\xi^2 A - \Omega\,A\,\ln|A|. \tag{21}$$

Indeed, if A denotes a nonvanishing solution of (21) then Ansatz (14) provides a residual error $E = \mathcal{O}((p-2)^{3/2})$ (substitute expansion (13) and $|A|^{p-2} = 1 + \mathcal{O}(p-2)$ in (20)).

As an alternative to (21), one can consider the following p-dependent fully nonlinear NLS equations

$$i\partial_\tau A = \cos q\,(\partial_\xi^2 A)\,|A|^{p-2} - \Omega\,N_p(A), \tag{22}$$

$$i\partial_\tau A = \cos q\,\partial_\xi^2(A\,|A|^{p-2}) - \Omega\,N_p(A) \tag{23}$$

(the log-NLS equation corresponds to leading order terms in (22), (23) when $p \to 2^+$). If A denotes a nonvanishing solution of (22) or (23) bounded independently of p, then Ansatz (14) yields $E = \mathcal{O}((p-2)^{3/2})$ when $p \to 2^+$.

Remark 2.1. *Equation (23) could be derived more straightforwardly using the relative variables $b_n = a_n - a_{n-1}$ (see* [2] *for a similar discussion in the case of Hertzian solitary waves).*

As we shall see in section 33.2, equations (21)-(23) possess some explicit stationary solutions which are strongly localized in space in the focusing case $q \in (\frac{\pi}{2}, \pi]$. These solutions consist of a Gaussian for equation (21) and compactons for equations (22), (23), and provide approximate traveling (or static) breather solutions of (4). Their strong spatial localization (faster than exponential) is due to the singular logarithmic nonlinearity in (21), and to a vanishing dispersion in the limit of zero amplitude in the case of systems (22), (23). The superexponential localization of approximate solutions is in good agreement with results established in [34] for exact static breathers solutions of (4).

Remark 2.2. *The more classical (and p-dependent) NLS equation*

$$i\partial_\tau A = \cos q\, \partial_\xi^2 A - \Omega\, N_p(A) \tag{24}$$

yields also $E = \mathcal{O}((p-2)^{3/2})$. However, its localized stationary solutions decay only exponentially at infinity, albeit at a fast rate $\mathcal{O}((p-2)^{-1/2})$. Due to this loss of superexponential localization, we shall not resort to equation (24) in the present study.

Remark 2.3. *Given a sufficiently smooth solution of (21), (22) or (23), we have shown that $E = \mathcal{O}((p-2)^{3/2})$ whenever $A(\xi,\tau) \neq 0$ is fixed and $p \to 2^+$. If $A(\xi,\tau) \approx 0$, the residue (19) is also small, roughly $\mathcal{O}(|A| + (p-2)^{1/2}|\partial_\xi A| + (p-2)|\partial_\tau A|)$.*

One can notice that $\|A(\cdot,\tau)\|_{L^2(\mathbb{R})}$ is a conserved quantity for equations (21), (22), (23) (originating from phase invariance), similar to the conserved quantity of (4)

$$P = \|a\|_{\ell_2(\mathbb{Z})}^2 = \sum_{n\in\mathbb{Z}} |a_n|^2.$$

Another interesting observation relates to Hamiltonian structure. The original system (4) is Hamiltonian, with energy

$$H = \frac{2}{p} \sum_{n\in\mathbb{Z}} |a_{n+1} - a_n|^p.$$

Preservation of this Hamiltonian structure is not automatic, except if one uses specific derivation procedures [55, 27]. The log-NLS equation is Hamiltonian, since it can be formally written $\partial_\tau A = i\, D_{\bar{A}}\mathcal{H}$ with

$$\mathcal{H} = \int_{\mathbb{R}} \cos q\, |\partial_\xi A|^2 + \frac{\Omega}{2}\, |A|^2\, (\ln |A|^2 - 1)\, d\xi.$$

Remark 2.4. *There exists an Hamiltonian amplitude equation $\partial_\tau A = i\, D_{\bar{A}}\tilde{\mathcal{H}}$ taking the form of a fully nonlinear NLS equation similar to (22) and (23) and leading to $E = \mathcal{O}((p-2)^{3/2})$. The Hamiltonian reads*

$$\tilde{\mathcal{H}} = \int_{\mathbb{R}} \cos q\, |\partial_\xi A|^2\, |A|^{p-2} + \frac{\Omega}{p-2}\, (\frac{2}{p}|A|^p - |A|^2)\, d\xi,$$

leading to the dynamical equation

$$i\partial_\tau A = \cos q\, (\partial_\xi^2 A)\, |A|^{p-2} + (p-2)\, \frac{\cos q}{2}\, (\partial_\xi A)^2 \bar{A}\, |A|^{p-4} - \Omega\, N_p(A).$$

3. Analytical approximations of traveling breathers and solitary waves

3.1. **Equivalent characterizations.** Exact traveling breathers are spatially localized solutions of (4) satisfying

$$e^{i\,\theta}\,a_{n+1}(t+\frac{1}{v})=a_n(t),\quad \forall n\,\in\,\mathbb{Z},\quad \forall t\,\in\,\mathbb{R} \tag{25}$$

for some parameters $v\neq 0$ (the breather velocity) and $\theta\in\mathbb{R}/(2\pi\mathbb{Z})$ ($-\theta$ corresponds to the breather phase shift after it propagates from one site to the next). If $\theta=0(2\pi)$, the solution corresponds to a solitary wave.

Equation (25) is equivalent to

$$e^{i\,\theta}\,a_{n+1}(1/v)=a_n(0),\quad \forall n\,\in\,\mathbb{Z}. \tag{26}$$

Indeed, if (26) holds true, then both sides of (25) define solutions of (4) which coincide at $t=0$, and thus are equal for all $t\,\in\,\mathbb{R}$. Characterization (26) will be used in section 4 to compute traveling breathers numerically.

Rewriting (25) as $a_n(t)=e^{-i\,\theta}\,a_{n-1}(t-\frac{1}{v})$ and proceeding by induction, we find that (25) is equivalent to

$$a_n(t)=a_0(t-\frac{n}{v})\,e^{-i\,\theta\,n},\quad \forall n\,\in\,\mathbb{Z}, \tag{27}$$

and $a_n(t)$ defines a traveling breather solution provided a_0 decays to 0 at infinity. It can be convenient to rewrite (27) in the form

$$a_n(t)=A_0(t-\frac{n}{v})\,e^{i(\omega\,t-q\,n)}, \tag{28}$$

with $A_0(t)=a_0(t)\,e^{-i\,\omega\,t}$ and q,ω linked by the identity

$$q=\theta+\frac{\omega}{v}\,(2\pi). \tag{29}$$

In section 3.2, we shall compute approximate traveling breather solutions taking the form (28) using the amplitude equations derived in section 2 in the case $p\approx 2^+$. Section 3.3 will address the approximation of solitary waves in the opposite limit when p is large. In both case we will compare the analytical approximations with numerical simulations of localized propagating waves excited by a localized perturbation. In section 3.4, additional qualitative properties of traveling breathers and solitary waves will be discussed in connection with the above findings.

3.2. **Approximate traveling breather solutions for $p\approx 2^+$.** From now on we consider the case when $q\in(\frac{\pi}{2},\pi]$. In that case, all the amplitude equations derived in section 2 admit stationary localized solutions described below. These solutions generate two-parameter families of approximate traveling breathers through Ansatz (14) when $p\approx 2^+$.

3.2.1. *Gaussian approximation.* The logarithmic NLS equation (21) admits Gaussian stationary solutions [5]

$$A_{\rm g}(\xi)=\sqrt{e}\exp\left(\frac{\Omega}{4\,\cos q}\,\xi^2\right). \tag{30}$$

With Ansatz (14), we obtain consequently approximate traveling breather solutions of (4) for $p\approx 2$

$$a_n^{\rm app}(t)=\sqrt{\frac{e}{\Omega}}\,R\,e^{i\,(\Omega\,|R|^{p-2}\,t-q\,n)}\exp\left(\frac{\Omega}{4\,\cos q}\,(p-2)\,(n-2\,\sin q\,|R|^{p-2}\,t)^2\right). \tag{31}$$

These traveling breathers are parameterized by their amplitude R and the wavenumber $q\in(\frac{\pi}{2},\pi]$ of the microscopic pattern. In particular, for $q=\pi$, the group velocity $c_q=2\,\sin q$ vanishes and the breathers become stationary.

3.2.2. *Compacton approximation from equation (23).* A stationary solution of (23) with compact support has been computed in [2] (this type of solution is called "compacton"). It can be obtained by setting $A(\xi) = B^{\frac{1}{p-1}}\left((\frac{\Omega}{(p-2)\,|\cos q|})^{1/2}\,\xi\right)$ in (23) (assuming $A, B \geq 0$), which yields

$$B'' + B - B^{r-1} = 0 \tag{32}$$

with $r = p/(p-1) \in (1,2)$. Integrating (32) leads to the equation $(B')^2 + B^2 = \frac{2}{r}\,B^r$, which admits the solution

$$B(\xi) = \left(\frac{r}{2}\right)^{\frac{1}{r-2}}\,\cos^{\frac{2}{2-r}}\left((1-\frac{r}{2})\xi\right) \tag{33}$$

defined for $|\xi|(1-\frac{r}{2}) \leq \pi/2$. This yields the compacton solution of (23)

$$A_{\rm c}(\xi) = \begin{cases} A_1 \cos^{\frac{2}{p-2}}(\lambda\xi), & |\xi| \leq \frac{\pi}{2\lambda}, \\ 0, & |\xi| \geq \frac{\pi}{2\lambda}, \end{cases} \tag{34}$$

with

$$A_1 = \left(\frac{p}{2(p-1)}\right)^{\frac{1}{2-p}}, \quad \lambda = \frac{1}{2(p-1)}\,\sqrt{\frac{\Omega(p-2)}{|\cos q|}}.$$

With Ansatz (14), we obtain approximate traveling breather solutions of (4) with compact support

$$a_n^{\rm app}(t) = \frac{R}{\sqrt{\Omega}}\,e^{i\,(\Omega\,|R|^{p-2}\,t - q\,n)}\,A_{\rm c}[\sqrt{p-2}\,(n - 2\,\sin q\,|R|^{p-2}\,t)]. \tag{35}$$

We note that $\lim_{p\to 2} A_1 = \sqrt{e}$, and one has for all fixed $\xi \in \mathbb{R}$

$$\begin{aligned} \cos^{\frac{2}{p-2}}(\lambda\xi) &= \exp\left(\frac{2}{p-2}\,\ln\left[1 - \lambda^2\xi^2/2 + \mathcal{O}((p-2)^2)\right]\right) \\ &\to \exp\left(\frac{\Omega}{4\,\cos q}\,\xi^2\right) \text{ when } p \to 2. \end{aligned}$$

It follows that $\lim_{p\to 2} A_{\rm c}(\xi) = A_{\rm g}(\xi)$ for all fixed $\xi \in \mathbb{R}$. Consequently, the compacton approximation (35) and the Gaussian approximation (31) become close when $p \to 2^+$.

3.2.3. *Compacton approximation from equation (22).* In the stationary case (and for $A \geq 0$), equation (22) can be recast in the form (32) with $r = 4-p$, setting $A(\xi) = B\left((\frac{\Omega}{(p-2)\,|\cos q|})^{1/2}\,\xi\right)$. We further assume $p \in (2,4)$, so that $r \in (0,2)$. From the solution (33) of equation (32) (defined for $|\xi|(1-\frac{r}{2}) < \pi/2$) we obtain the solution of (22)

$$\tilde{A}_{\rm c}(\xi) = \begin{cases} \tilde{A}_1 \cos^{\frac{2}{p-2}}(\tilde{\lambda}\xi), & |\xi| \leq \frac{\pi}{2\tilde{\lambda}}, \\ 0, & |\xi| \geq \frac{\pi}{2\tilde{\lambda}}, \end{cases} \tag{36}$$

where

$$\tilde{A}_1 = \left(2 - \frac{p}{2}\right)^{\frac{1}{2-p}}, \quad \tilde{\lambda} = \frac{1}{2}\,\sqrt{\frac{\Omega(p-2)}{|\cos q|}}.$$

Note that equation (22) must be interpreted with caution when $p \in [3,4)$, because $\tilde{A}_{\rm c}''$ is singular at $\xi = \pm\frac{\pi}{2\tilde{\lambda}}$ (piecewise continuous for $p = 3$ and unbounded for $3 < p < 4$) but $\tilde{A}_{\rm c}''\,\tilde{A}_{\rm c}^{p-2}$ is C^1.

As previously one can check that $\lim_{p\to 2} \tilde{A}_{\rm c}(\xi) = A_{\rm g}(\xi)$ for all fixed $\xi \in \mathbb{R}$. Ansatz (14) yields approximate traveling breather solutions of (4) with compact support

$$a_n^{\rm app}(t) = \frac{R}{\sqrt{\Omega}}\,e^{i\,(\Omega\,|R|^{p-2}\,t - q\,n)}\,\tilde{A}_{\rm c}[\sqrt{p-2}\,(n - 2\,\sin q\,|R|^{p-2}\,t)]. \tag{37}$$

3.2.4. *Comparison with a dynamical simulation.* In this section, we illustrate the excitation of a traveling breather from a localized perturbation in system (4). Numerical computations are performed for a long chain ($1 \leq n \leq 1500$) and free-end boundary conditions. We set $p = 2.1$ and consider the initial condition $a_n(0) = 0$ for $n \geq 2$ and $a_1(0) = -i$. This perturbation generates a traveling breather whose profile will be compared to the analytical approximations derived above for $p \approx 2^+$. Throughout this paper, time-integrations of (4) are performed using the standard ODE solver of the software package Scilab.

Figure 2 illustrates the evolution of $a_n(t)$ under the DpS equation (4). One can notice a robust propagating localized mode (traveling breather) followed by a weak and fairly extended "wake". The traveling breather propagates almost steadily, with the amplitude of the main pulse (i.e. supremum of $|a_n(t)|$ over time) decaying by only 0.12% after it travels over 100 sites from $n = 1280$. Its velocity is $v \approx 1.51$ and its phase $\theta \approx 0.31$. The wake consists of dispersive wave trains having a rather complex structure, clearly separated from the breather by a (weakly modulated) sinusoidal tail of very small amplitude. This tail is close to a periodic traveling wave solution of (4), as we will see in more detail in section 3.4-3.4.2).

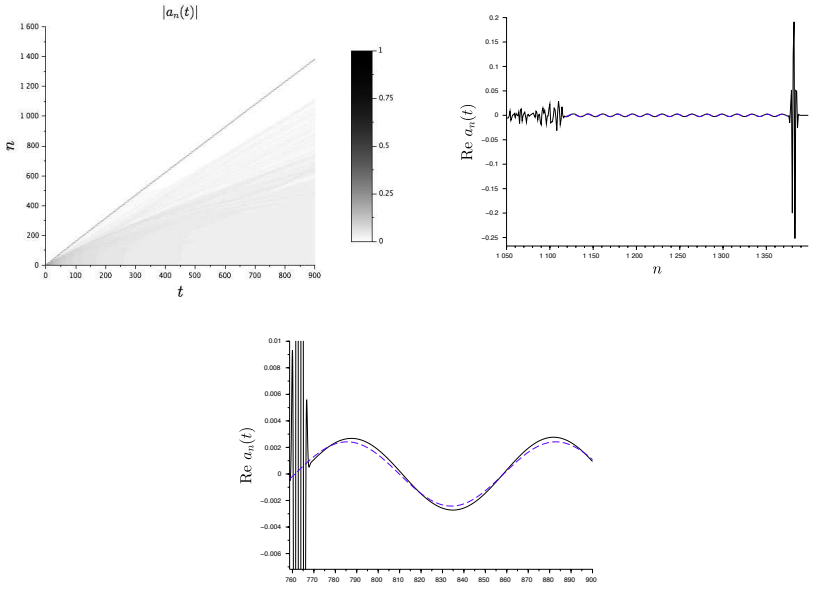

FIGURE 2. Top left plot : space-time evolution of $|a_n(t)|$ for system (4) with $p = 2.1$, free-end boundary conditions and an initial condition localized on the first particle ($a_1(0) = -i$, $a_n(0) = 0$ for $n \geq 2$). Top right plot : spatial profile of $\mathrm{Re}\, a_n(t)$ at $t = t_0 = 900$ (black line). The traveling breather is followed by a tail close to a sinusoid which extends over 257 sites. Within this region behind the breather, one has $\mathrm{Re}\, a_n(t) \approx \rho \cos(k(n - n_0))$, with $\rho \approx 0.0024$, $k \approx 0.36$, $n_0 = 1351$. This sinusoidal approximation is represented by the dashed blue line. Lower plot : time-evolution of $\mathrm{Re}\, a_n(t)$ at $n = 1175$ after the passage of the moving breather (black line), and comparison with the sinusoidal approximation $\mathrm{Re}\, a_n(t) \approx \rho \cos\left(\omega_{\mathrm{tw}}(t - t_0) - k(n - n_0)\right)$ with $\omega_{\mathrm{tw}} = \rho^{p-2}(2 \sin(k/2))^p \approx 0.065$ (dashed blue line).

Let us now compare the traveling breather profile with the approximate traveling breather solutions (31), (35) and (37). These approximations take the form (28) with

$$v = 2 \sin q\, |R|^{p-2} \tag{38}$$

and $\omega = 4\sin^2(q/2)|R|^{p-2}$. Using (29), their phase θ satisfies consequently

$$q - \tan(q/2) = \theta\,(2\pi). \tag{39}$$

Using the values of θ and v computed from the numerical simulation, we get $q \approx 2.142$ from (39) and $R \approx 0.34$ from (38). Figure 3 compares the three resulting analytical approximations to the outcome of the numerical simulation. The relative error between numerical solution and analytical approximations (supremum norm for $t \in [862, 882]$, normalized by the breather amplitude) is 11.6% for the Gaussian approximation (31) (blue curve), 11.8% for the compacton (37) (green curve) and 13% for the compacton (35) (black curve). The error on the traveling breather amplitude is much smaller, 0.024% for the Gaussian approximation (31), 1.3% for the compacton (37) and 3.4% for the compacton (35). The comparison is thus quite satisfactory given the additional errors induced by the determination of parameters θ and v and the fact that the moving breather has not yet reached a fully steady regime. A more precise comparison will be made in section 4, where exact traveling breathers will be computed more precisely using an iterative method, and values of p closer to 2 will be considered as well.

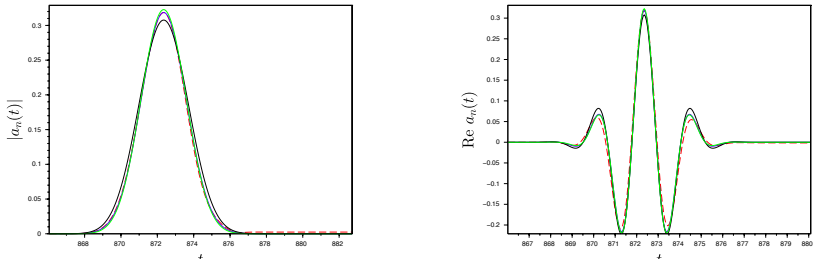

FIGURE 3. Time-evolution of $|a_n(t)|$ (left plot) and $\mathrm{Re}\,(a_n(t))$ (right plot) during the passage of the moving breather at $n_1 = 1340$. The red dashed lines correspond to the numerical simulation of figure 2. In the right panel we have applied an appropriate phase shift, i.e. we plot $\mathrm{Re}\,(a_n(t)\,e^{i\,\varphi})$ with $\varphi = -0.3$. These profiles are compared with the analytical approximations $a^{\mathrm{app}}_{n-n_1}(t - t_1)$ obtained for $p \approx 2^+$, where we set $n = n_1$, $t_1 = 872.35$, $q \approx 2.142$, $R \approx 0.34$ and $p = 2.1$. The blue line corresponds to the Gaussian approximation (31), the black line to the compacton approximation (35), and the green line to the compacton approximation (37).

3.3. **Solitary waves for p large.** In order to investigate the "vibroimpact" limit corresponding to large values of p, we start by simulating the evolution of a localized perturbation in a chain of 330 particles with free-end boundary conditions. We set $a_n(0) = 0$ for $n \geq 2$ and $|a_1(0)| = 1$. When p is large, one observes after a short transient the formation of a solitary wave with velocity v close to $2/\pi$ (see figure 4). The solitary wave is strongly localized (mainly on two lattice sites) and is followed by a small and quasi-stationary tail (see the lower plot of figure 4). The tail amplitude decays relatively slowly with increasing n (it is $O(1/n)$). We observe a convergence of the propagating pulse towards a limiting profile $a_n(t) = y(n - v\,t)$ when $p \to +\infty$ (the limiting profile is described in figure 5). Due to the phase invariance $a_n(t) \to a_n(t)\,e^{i\,\varphi}$ of (4), this profile is unique up to a factor $e^{i\,\varphi}$ determined by the phase of the initial localized perturbation.

Remark 3.1. *Due to the scaling invariance $a_n(t) \to R\,a_n(|R|^{p-2}\,t)$ of (4), choosing $|a_1(0)| = R$ results in $v \sim 2\,R^{p-2}/\pi$ when p is large, hence one generates slow or fast solitary waves depending whether $R < 1$ or $R > 1$.*

We describe below a heuristic method which allows to approximate the limiting solitary wave profile and velocity v. We consider an infinite chain ($n \in \mathbb{Z}$) and look for solitary waves $a_n(t) = y(\xi)$ with $\xi = n - v\,t$ ($v \neq 0$) and $\lim_{\xi\to\pm\infty} y(\xi) = 0$. Equation (4) reduces to

$$-i\,v\,y'(\xi) = f(\xi+1) - f(\xi) \tag{40}$$

where

$$f = B|B|^{p-2}, \quad B(\xi) = y(\xi) - y(\xi-1). \tag{41}$$

Remark 3.2. *Front solutions satisfying* $\lim_{\xi\to\pm\infty} y(\xi) = c_\pm$ *for some constants* $c_+ \neq c_-$ *do not exist for the DpS equation. Indeed, integrating (40) yields* $-i\,v\,y(\xi) = c + \int_\xi^{\xi+1} f(s)\,ds$ *for some constant* c*. If* y *admits two finite limits* $c_\pm$ *at* $\pm\infty$*, which implies vanishing of* f *at infinity, we have then* $\lim_{\xi\to\pm\infty} y(\xi) = c$*, i.e.* $c_+ = c_- = c$*. This property of the (translation-invariant, first order) DpS equation contrasts with the case of the (translation-invariant, second order) FPU model. In the case of FPU solitary waves* [28] *(in particular with Hertzian potentials* [2]*), it is known that particle displacements correspond to fronts connecting constant displacement fields at infinity, and relative displacements decay to* 0 *at infinity.*

Upon rescaling v, one can restrict (40)-(41) to solutions satisfying $\|B\|_\infty = 1$. In that case, letting $p \to +\infty$ yields *formally* the following limit problem

$$-i\,v\,y'(\xi) = B(\xi+1)\,\mathbf{1}_{|z|=1}(B(\xi+1)) - B(\xi)\,\mathbf{1}_{|z|=1}(B(\xi)), \tag{42}$$

where $\mathbf{1}_{|z|=1}$ denotes the characteristic function of the unit circle in $\mathbb{C}$, y is assumed absolutely continuous and (42) holds true almost everywhere.

We shall not attempt to justify approximation (42) rigorously. Instead, we explicitly compute a family of localized solutions of (42), and we check numerically that one of them correctly approximates the propagating pulse.

We look for solutions of (42) having the following structure :

$$|B| = 1 \text{ on } [0,1], \quad |B| < 1 \text{ almost everywhere in } (-\infty,0) \cup (1,+\infty). \tag{43}$$

In conjunction with (42), this assumption leads to $y' = 0$ a.e. in $(-\infty,-1) \cup (1,+\infty)$, and thus $y(\xi) = 0$ for $|\xi| \geq 1$ for a solitary wave decaying to 0 at infinity. This property is consistent with the observed localization of the traveling pulse on two lattice sites when $p \to +\infty$.

Assumption (43) and equation (42) lead to $\frac{d}{d\xi}(y(\xi) + y(\xi-1)) = 0$ a.e. in $(0,1)$, hence there exists $\mu \in \mathbb{C}$ such that

$$y(\xi) + y(\xi-1) = \mu \quad \text{for all } \xi \in [0,1]. \tag{44}$$

It follows that $B = 2y - \mu$ on $[0,1]$, which implies $|\mu| = 1$ (since $|B(1)| = 1$ and $y(1) = 0$). Due to the invariance $y \to y\,e^{i\,\varphi}$ of (42), one can fix $\mu = 1$ without loss of generality. Then we infer from (42) :

$$i\,v\,y' = 2\,y - 1 \quad \text{a.e. on } (0,1). \tag{45}$$

Recalling that $y(\pm 1) = 0$ and using (44), equation (45) is supplemented by the boundary conditions

$$y(0) = 1, \quad y(1) = 0. \tag{46}$$

Solving (45)-(46) leads to $v = 2/((2k+1)\,\pi)$ ($k \in \mathbb{Z}$) and

$$y(\xi) = \frac{1}{2}\,(1 + e^{-i\,(2k+1)\,\pi\,\xi})\,\mathbf{1}_{[-1,1]}(\xi), \tag{47}$$

where we have used (44) to compute $y_{|[-1,0]}$ from $y_{|[0,1]}$. One can check that assumption (43) is consistently satisfied by (47), hence (47) defines a solution of (42) for all $k \in \mathbb{Z}$. Returning

to the original variable $a_n(t)$ and fixing $k = 0$ in (47), one obtains the following approximate solution of (4) when p is large :

$$\tilde{a}_n^{\rm app}(t) = \frac{1}{2}\,\big(\,1 + (-1)^n\, e^{2\,i\,t}\,\big)\,\mathbf{1}_{[-1,1]}\big(\,n - \frac{2\,t}{\pi}\,\big). \tag{48}$$

Taking into account symmetries of (4), this provides a more general family of approximate solitary wave solutions

$$a_n(t) \approx e^{-i\,\varphi}\,\tilde{a}^{\rm app}_{n-n_0}(t - t_0) + c, \tag{49}$$

where $\varphi \in \mathbb{R}/(2\pi\mathbb{Z})$, $n_0 \in \mathbb{Z}$, $t_0 \in \mathbb{R}$ and $c \in \mathbb{C}$ are arbitrary constants. As illustrated by figure 5, this approximation is very close to the traveling pulse computed numerically for large p, for appropriate choice of parameters φ, n_0, t_0 and $c = 0$.

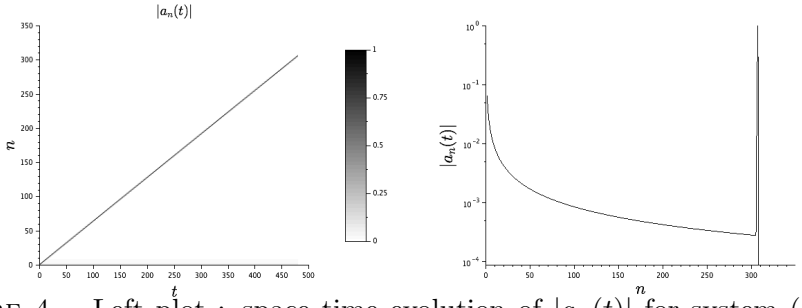

FIGURE 4. Left plot : space time evolution of $|a_n(t)|$ for system (4) with p large, free-end boundary conditions and an initial condition localized on the first particle ($a_1(0) = -i$, $a_n(0) = 0$ for $n \geq 2$). We have fixed $p = 201$ in the numerical simulation. One observes a solitary wave with velocity $v \approx 0.63 \approx 2/\pi$. Right plot : spatial profile of $|a_n(t)|$ at $t = 479.84$ (semi-logarithmic scale).

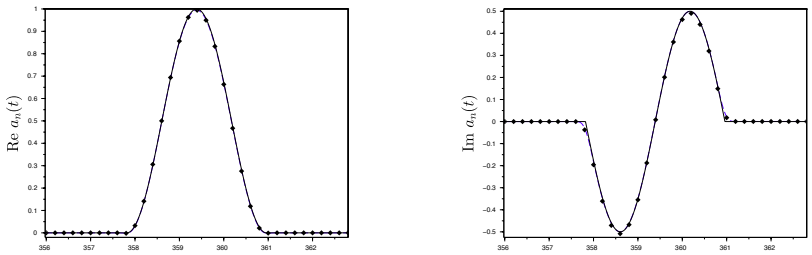

FIGURE 5. Real part (left plot) and imaginary part (right plot) of the traveling pulse when p is large. The dashed blue line corresponds to $e^{i\,\varphi}\,a_{n_0}(t)$, where $a_n(t)$ denotes numerical solution obtained in figure 4 for $p = 201$, $n_0 = 230$ and $\varphi \approx 2$. Dots correspond to $e^{i\,\varphi}\,a_{n_1}(t + \Delta t)$ with $n_1 = 270$ and $\Delta t = 63$. The graphs obtained with $n = n_0$ and $n = n_1$ coincide almost perfectly, illustrating the steady wave propagation at velocity $v \approx 2/\pi \approx (n_1 - n_0)/\Delta t$. The full black line correspond to analytical approximation (49) appropriately shifted in time and space (we plot $\tilde{a}_0^{\rm app}(t - t_0)$ with $t_0 = 359.39$). One observes that this approximation is extremely close to the numerical solution.

3.4. **Additional qualitative properties of traveling breathers.**

3.4.1. *A constraint on exact traveling breather solutions.* Let us consider the evolution problem (4) in $\ell_1(\mathbb{Z})$ (the Banach space of summable sequences). Equation (4) admits the conserved quantity $\mathcal{S} = \sum_{n\in\mathbb{Z}} a_n(t)$ which originates from translational invariance (an analogous result holds true with periodic boundary conditions). This conserved quantity induces a constraint on traveling breather solutions satisfying $a(t) \in \ell_1(\mathbb{Z})$. Indeed, the conservation of $\mathcal{S}$ and property (25) lead to

$$\sum_{n\in\mathbb{Z}} a_n(t) = \sum_{n\in\mathbb{Z}} a_n(t+\frac{1}{v}) = e^{-i\,\theta} \sum_{n\in\mathbb{Z}} a_n(t), \tag{50}$$

therefore we have for $\theta \neq 0\,(2\pi)$

$$\sum_{n\in\mathbb{Z}} a_n(t) = 0. \tag{51}$$

In what follows we evaluate the constraint (51) for the approximate traveling breather solutions $a_n^{\rm app}$ obtained in section 3.2 when $p \to 2^+$. We fix $q \in (\pi/2, \pi)$ and consider the Gaussian approximation (31) for simplicity. Using Poisson's summation formula and identity (29), one obtains after some algebraic manipulations

$$\mathcal{S}^{\rm app}(t) := \sum_{n\in\mathbb{Z}} a_n^{\rm app}(t) = \frac{R}{\sqrt{(p-2)\Omega}}\, e^{-i\,v\,\theta\,t} \sum_{m\in\mathbb{Z}} e^{-2i\pi\,v\,t\,m}\, \hat{A}_{\rm g}\big(\frac{1}{\sqrt{p-2}}(m+\frac{q}{2\pi})\big),$$

where $\hat{A}_{\rm g}$ denotes the Fourier transform of (30). This yields after lengthy but straightforward computations

$$\|\mathcal{S}^{\rm app}\|_\infty \sim \frac{2R}{\Omega}\sqrt{\pi\, e\,|\cos q|}\,\frac{1}{\sqrt{p-2}}\exp\left(\frac{q^2\cos q}{(p-2)\,\Omega}\right) \tag{52}$$

when $p \to 2^+$. Consequently, the constraint (51) is almost satisfied by Ansatz (31) when $p \to 2^+$, up to an exponentially small error given by (52).

Remark 3.3. *Solitary waves need not satisfy (51) (case $\theta = 0(2\pi)$). For example, with the approximate solitary wave solution (48) obtained when p is large, one finds*

$$\sum_{n\in\mathbb{Z}} \tilde{a}_n^{\rm app}(t) = 1 \quad \textit{for all } t \in \mathbb{R}$$

after some simplifications (the sum contains only two nonvanishing terms).

3.4.2. *Traveling breathers with oscillatory tails.* In standard periodic nonlinear lattices (i.e. excluding "sonic vacua" where the linearized equations do not support phonon waves), exact traveling breathers are generally superposed on nondecaying oscillatory tails lying at both sides of the main pulse. This phenomenon has been mathematically analyzed in a number of works (see e.g. [29, 62, 30, 52] and references therein) and the corresponding solutions are often referred to as "generalized" traveling breathers or solitary waves, or "nanopterons" (thereafter we shall use the denomination "traveling breather" independently of the presence or absence of a nondecaying oscillatory tail). The tails are close to a linear phonon (or a superposition thereof) whose wavenumber q and frequency ω satisfy a resonance condition reminiscent of (29) [21, 30]. Typically the tail amplitude can vary freely in some interval, with a lower bound exponentially small compared to the main pulse at small amplitude, a limit in which the wave becomes loosely localized (see e.g. [30] and references therein). In generic models, the tail may exactly vanish only under special choices of the speed of the traveling breather (or the system parameters) [47, 48]. In connection with the above phenomena, traveling breathers excited from localized initial perturbations are often followed by a small oscillatory tail, see e.g. [32, 69] in the context of granular crystals.

Part of the above phenomenology can be transposed to the present setting despite the fact that equation (4) is fully nonlinear. Indeed, instead of weakly modulated phonons, the tails can involve nonlinear periodic traveling waves of (4) taking the form [31]

$$a_n(t) = \rho\, e^{i\,(\Omega^{p/2}(k)\,\rho^{p-2}\,t - k\,n + \varphi)}, \tag{53}$$

where $\Omega(k) = 4\sin^2(k/2)$. These solutions are parameterized by the wavenumber k, amplitude $\rho > 0$ and phase φ (expression (53) can be obtained by setting $A = 1$ and $R = \rho\sqrt{\Omega}$ in (14)). These periodic waves (or slow modulations thereof) are good candidates to approximate oscillatory tails of exact traveling breathers when $n \to \pm\infty$, or to describe the small oscillations emitted at the rear of (non-stationary) moving breathers generated from localized perturbations.

In order for a "resonant" traveling wave to match (25), the wavenumber k and amplitude ρ must satisfy the compatibility condition

$$k - \frac{1}{v}\Omega^{p/2}(k)\,\rho^{p-2} = \theta\,(2\pi). \tag{54}$$

From equation (54), ρ can be expressed as a function of k (except for the trivial branch $a_n(t) = \rho\, e^{i\,\varphi}$ if $\theta = 0\,(2\pi)$), therefore resonant periodic traveling waves form a one-parameter family parameterized by k. In particular, ρ is close to 0 when $\theta \neq 0\,(2\pi)$ and k lies slightly above θ.

In connection with the above observation, let us now examine more closely the numerical simulation of section 3.2-3.2.4) performed for $p = 2.1$. We recall that the traveling breather excited by a localized perturbation satisfies $v \approx 1.51$, $\theta \approx 0.31$ and is followed by a small oscillatory tail of amplitude close to $\rho \approx 0.0024$. In the tail region, one observes that $a_n(t)$ is close to the periodic wave (53) with $k \approx 0.36$ and an appropriate phase φ (see figure 2). This leads to $k - \frac{1}{v}\Omega^{p/2}(k)\,\rho^{p-2} \approx 0.32$ which is close to θ, hence the compatibility condition (54) is almost satisfied. Note that a perfect match cannot be expected because the tail is actually weakly modulated and the traveling breather slightly non-stationary.

Another manifestation of the above phenomenology will be illustrated in section 4, where we compute traveling breathers iteratively for a wide range of parameter values. These computations reveal oscillatory tails with a rather wide range of amplitudes and wavenumbers. In particular, we find traveling breathers with very small tails (compared to the amplitude of the main pulse) and k close to θ, which is consistent with the case $\rho \approx 0$ of equation (54). Preliminary computations also indicate that the tail amplitude can become exponentially small when p is close to 2 (see section 44.2), a limit leading to traveling breathers with a large spatial extent. However, we will not attempt to compute the minimal tail size for given parameter values, and in particular to determine if the tail may *exactly* vanish or not (these problems are quite delicate and out of the scope of the present study).

4. Newton-type computations

In this section we compute exact traveling breather solutions of (4) iteratively and compare the numerical solutions to the approximations of section 33.2.

4.1. **Numerical method.** Any initial condition $a(0) = a^0 \in \ell_1(\mathbb{Z})$ determines a unique solution of (4) denoted by $a_n(t) = \Phi_n(t; a^0)$. Our aim is to compute initial conditions a^0 corresponding to traveling breather solutions. We fix two parameters $\theta \in \mathbb{R}/(2\pi\mathbb{Z})$, $v > 0$ and look for solutions satisfying (26). One can fix $v > 0$ without loss of generality due to the invariance $n \to -n$ of (4). From equation (26), searching for exact traveling breather solutions reduces

to finding zeros $a^0 \in \ell_1(\mathbb{Z})$ of the nonlinear map $F_{\theta,v} : \ell_1(\mathbb{Z}) \to \ell_1(\mathbb{Z})$ defined by

$$[F_{\theta,v}(a^0)\,]_n = e^{i\,\theta}\,\Phi_{n+1}(\frac{1}{v};a^0) - a_n^0.$$

Note also that $\Phi_n(t;R\,a^0) = R\,\Phi_n(|R|^{p-2}t;a^0)$ due to the scale invariance of (4). We have thus

$$F_{\theta,v}(a^0) = 0 \iff F_{\theta,v|R|^{p-2}}(R\,a^0) = 0, \tag{55}$$

i.e varying breather velocity is equivalent to rescaling its amplitude.

In our numerical computations, the infinite chain is replaced by a periodic chain with N particles and $F_{\theta,v}$ translates to a map in $\mathbb{C}^N$, whose zeros can be computed iteratively. The zeros of $F_{\theta,v}$ are not isolated due to the invariance of (4) under time shift and the phase invariance $a_n \to a_n\,e^{i\,\phi}$. Moreover, in the particular case $\theta = 0\,(2\pi)$ corresponding to traveling waves, the translational invariance $a_n \to a_n + d$ ($d \in \mathbb{C}$) yields additional degeneracy. To remove degeneracies due to invariances under time and phase shifts, we exploit the existence of a reversibility symmetry $a_n(t) \to \bar{a}_n(-t)$ and reflectional symmetry $a_n \to a_{-n}$ for (4). More precisely, we restrict our attention to reversible traveling breather solutions satisfying $a_n(t) = \bar{a}_{-n}(-t)$, which is equivalent to fixing $a_n^0 = \bar{a}_{-n}^0$. In addition, we impose $\sum_n a_n^0 = 0$ in order to match the constraint (51) for localized traveling breathers and to remove degeneracy due to translational invariance when $\theta \to 0$. Fixing N odd, the set $\mathcal{S} \subset \mathbb{C}^N$ of symmetric zero-mean initial conditions a^0 is isomorphic to $\mathbb{C}^{(N-1)/2}$.

We use the Gauss-Newton method [7] to minimize $\|F_{\theta,v}\|_2$ on $\mathcal{S}$ (time integrations are performed using Scilab). The relative residual error for the last (k-th) Newton iteration satisfies in all cases

$$\epsilon_{\rm res} = \frac{\|F_{\theta,v}(a^0(k))\|_\infty}{\|a^0(k)\|_\infty} < 10^{-9},$$

and the incremental error (relative variation of the last two iterates) always satisfies

$$\epsilon_{\rm inc} = \frac{\|a^0(k) - a^0(k-1)\|_\infty}{\|a^0(k)\|_\infty} < 10^{-9}. \tag{56}$$

The number of particles must be fixed relatively large due to the broadening of the breathers when $p \to 2$ (see section 33.2). More generally, it is interesting to consider a large number of particles in order to be closer to the case of an infinite lattice. Indeed, the numerical iteration tends to converge towards traveling breathers with oscillatory tails, and one is able to capture a wider set of tail sizes when N is large.

A two-parameters family of traveling breather solutions of (4) can be computed by varying the breather velocity v and the phase θ in (26). We use the Gaussian approximation (31) to initiate the Gauss-Newton method with $a_n^{\rm app}(0)$ when p is close to 2. To select an approximate breather solution with given velocity v and phase $\theta \in \mathbb{R}/(2\pi\mathbb{Z})$, one has to determine Ansatz parameters q, R through system (38)-(39) which admits an infinity of solutions. Consequently, one can anticipate that the Gauss-Newton iteration may converge towards different traveling breather solutions depending on the choice of initial guess $a_n^{\rm app}(0)$ for a^0 (i.e. on the choice of q). From a practical point of view, we shall treat $q \in (\frac{\pi}{2},\pi)$ as a parameter and determine θ using (39). Once q is fixed, equation (38) determines the amplitude parameter R of Ansatz (31). In addition, the Ansatz (31) is appropriately translated in order to fulfill the constraint of zero mean.

Remark 4.1. *A classical approach to compute traveling wave or traveling breather solutions in lattices consists in solving a corresponding advance-delay differential equation (or an integral form thereof), using pseudospectral methods or high order quadrature formula for discretization*

and suitable iterative methods to handle the discretized nonlinear problem [37, 2, 28]. *For equation (4), setting* $a_n(t) = y(n - v\,t)\,e^{-i\,\theta\,n}$ *leads to*

$$-i\,v\,y'(\xi) = e^{-i\,\theta}\,f(\xi+1) - f(\xi) \tag{57}$$

where $f = B|B|^{p-2}$ *and* $B(\xi) = y(\xi) - e^{i\,\theta}\,y(\xi-1)$. *We do not use this approach because the right side of (57) is not* C^2 *everywhere when* $p \in (2,3)$, *which may lower the precision of the above numerical discretizations.*

4.2. **Continuation in p.** In this section we compare traveling breather solutions computed numerically and analytical approximations of section 33.2 when θ, v are fixed in (26) and p varies. In particular, we check that the relative errors between exact and approximate solutions decay to 0 (uniformly in time and space) when $p \to 2^+$. We fix $N = 499$ in our numerical computations.

Firstly, let us show that the breather velocity v can be normalized without loss of generality, which leaves only one free parameter θ in (26). Consider a traveling breather solution a_n satisfying (26) and an analytical approximation $a_n^{\rm app}$ of the form (14) (defined either by (31), (35) or (37)), with parameters q, R satisfying (38)-(39). One can write $a_n^{\rm app}(t) = R\,\tilde{a}_n^{\rm app}(|R|^{p-2}\,t)$, where $\tilde{a}_n^{\rm app}$ corresponds to the case $R = 1$ of (14). Similarly, setting $a_n(t) = R\,\tilde{a}_n(|R|^{p-2}\,t)$, we obtain a traveling breather solution $\tilde{a}_n$ of (4) satisfying (26) for $v = 2\sin q$ (due to property (55) and identity (38)). The relative error between numerical solution and analytical approximation satisfies

$$\frac{\sup\limits_{n\in\mathbb{Z},t\in\mathbb{R}} |a_n(t) - a_n^{\rm app}(t)|}{\sup\limits_{n\in\mathbb{Z},t\in\mathbb{R}} |a_n(t)|} = \frac{\|\tilde{a}_0 - \tilde{a}_0^{\rm app}\|_\infty}{\|\tilde{a}_0\|_\infty}, \tag{58}$$

where we have used property (27) satisfied by the traveling breather solution $\tilde{a}_n$ and the Ansatz $\tilde{a}_n^{\rm app}$. Consequently, one can restrict the error analysis to the case $v = 2\sin q$ of (26), where q and θ are linked by identity (39). We shall therefore fix $R = 1$ in the choice of the analytical approximation.

In what follows we fix $q = 3\pi/4$, which corresponds to $v = \sqrt{2}$ and $\theta = \frac{3\pi}{4} - 1 - \sqrt{2} \approx -0.058 \approx -9\pi/N$. Using the numerical procedure described in section 4.1, we study the evolution of the breather profile when p is varied in the interval $(2,4]$. The Gaussian approximation (31) is used to initiate the Newton iteration when $p < 3.1$ (since breather width varies strongly with p, path-following would require very small steps) and path following is used for larger values of p.

When p converges towards 2, the breather envelope becomes nearly Gaussian and breather solutions converge towards approximation (31) (see figures 6 and 7). As indicated in section 33.2, the Gaussian and the two compacton approximations become essentially equivalent in this regime (see figure 6). Discrepancies between the numerical and analytical profiles appear for larger values of p. For $p = 5/2$ (relevant case for Hertzian interactions), Gaussian approximation (31) and compacton approximation (35) yield a relative error around 14% in supremum norm, and compacton (37) yields a slightly larger error around 16%. Above $p = 2.9$, compacton approximation (37) becomes much less accurate than the Gaussian approximation (31) and compacton approximation (35). These two approximations are roughly of the same accuracy (see figures 6 and 8).

Spatial profiles of traveling breather solutions at $t = 0$ are represented in figures 9 and 10 for different values of p. A zoom at both sides of the breather center reveals the existence of small nondecaying oscillatory tails which are very close to sinusoids of the form $a_n = \pm i\,\rho\,e^{-i\,\theta\,n}$ at $t = 0$. This is consistent with the analysis of section 33.4-3.4.2), since the case $\rho \approx 0$ of (54) corresponds to $k \approx \theta$. Figure 11 describes the dependency in p of the tail amplitude ρ.

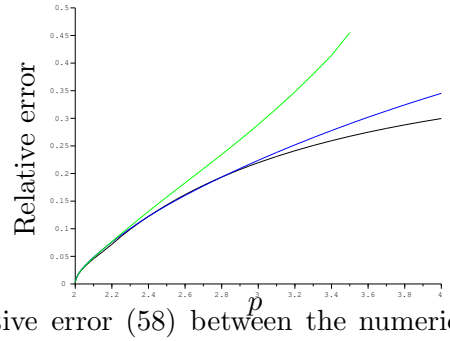

FIGURE 6. Relative error (58) between the numerical solution a (obtained for $v = \sqrt{2}$, $\theta \approx -0.058$) and the Gaussian approximation (31) (blue line), the compacton approximations (35) (black line) and (37) (green line) with $q = 3\pi/4$, $R = 1$. The error is plotted as a function of p. Note that $\|a_0\|_\infty$ has negligible variations when p varies in $(2, 4]$ ($\|a_0\|_\infty$ increases from 0.89 to 0.95).

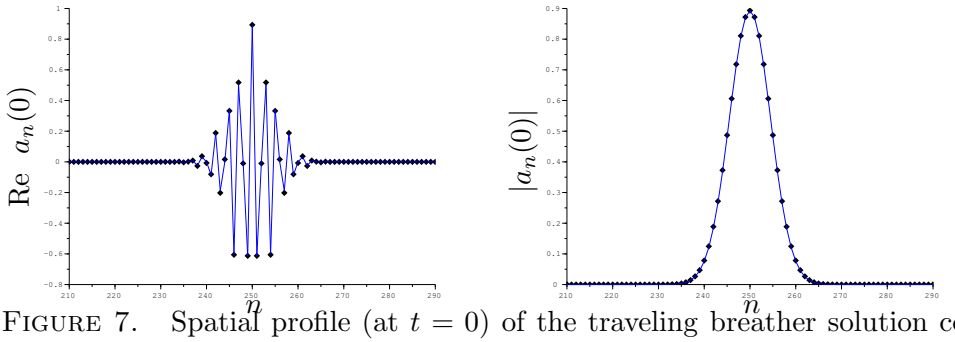

FIGURE 7. Spatial profile (at $t = 0$) of the traveling breather solution computed numerically in figure 6 in the case $p = 2.02$ (dots). This solution is compared with the Gaussian approximation (31) (blue line). The real part (left panel) and modulus (right panel) of the numerical solution and Gaussian approximation almost perfectly coincide.

For $p \in [2.1, 2.35]$ we find $\rho \propto e^{-c/(p-2)}$ with $c \approx 1.55$ (for smaller values of $p - 2$, the tail amplitude becomes comparable to the numerical error (56) so that tail computations are not reliable). By extrapolation this suggests that the minimal tail amplitude should lie beyond all orders when $p \to 2^+$ in an infinite chain. Another interesting question concerns the limit of the above numerical solution when lattice size goes to infinity and p is fixed. Tail size may vanish, leading to fully localized traveling breather solutions (this situation is non-generic in usual lattice models, as discussed in section 33.4-3.4.2)). Another possibility is the convergence of the numerical solution towards an heteroclinic solution connecting periodic traveling waves (53) satisfying the compatibility condition (54).

We have numerically tested for different values of p the robustness of the propagation of the traveling breathers computed by the Gauss-Newton method (data not shown). For this purpose one starts from the initial condition computed with the Newton method and one integrates (4) over long times (keeping the same periodic boundary conditions). For $p \leq 2.4$, we have obtained an almost perfect steady motion of the breather, traveling e.g. over 7500 lattice sites (the end of the simulation) for $p = 2.4$. As already noticed in [34], breather mobility decreases when p increases, but in our worst case ($p = 4$) the solution propagates steadily over 190 lattice sites before getting trapped.

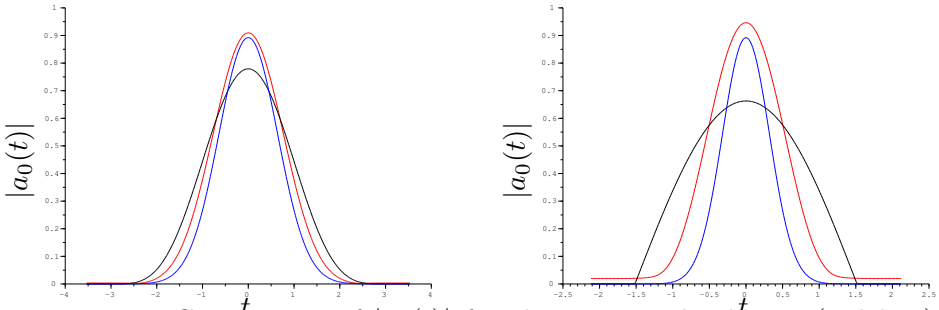

FIGURE 8. Comparison of $|a_0(t)|$ for the numerical solution (red line), the compacton approximation (35) (black line) and the Gaussian approximation (31) (blue line) of figure 6, when $p = 2.5$ (left) and $p = 4$ (right). Note that Gaussian approximation works better at the time of maximal amplitude while compacton approximation is more accurate (with respect to the uniform norm) in the steepest region.

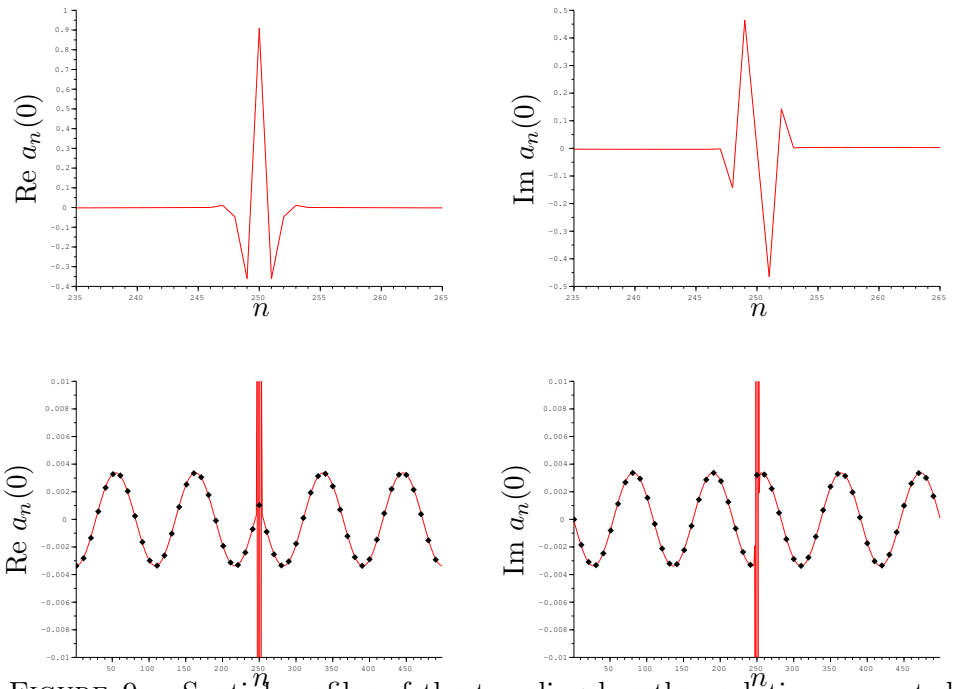

FIGURE 9. Spatial profiles of the traveling breather solution computed numerically in figure 6 in the case $p = 2.5$. The curves correspond to the real part (left panels) and imaginary part (right panels) of the numerical solution. Bottom panels display more lattice sites and provide a zoom at small amplitude, which reveals the existence of small nondecaying oscillatory tails at both sides of the moving breather. These tails are very close to sinusoids (dots) of the form $a_n = i\,\sigma\,\rho\,e^{-i\,\theta\,(n-n_0)}$ with $\rho = 0.00337$, $n_0 = 250$, $\sigma = \pm 1 = \mathrm{sign}(n - n_0)$.

4.3. **Continuation in (v, θ) at fixed energy.** In this section we fix $p = 5/2$ and numerically compute traveling breather solutions when θ and v vary in (26). Their values are determined by system (38)-(39), where $q \in (\frac{\pi}{2}, \pi)$ and R are free parameters. We use a shorter periodic

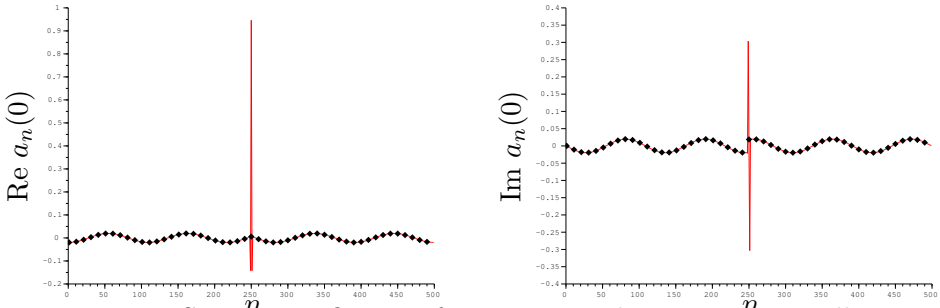

FIGURE 10. Same as in figure 9 for $p = 4$. In that case, the oscillatory tail is bigger ($\rho \approx 0.02$) and visible a the scale of the moving breather.

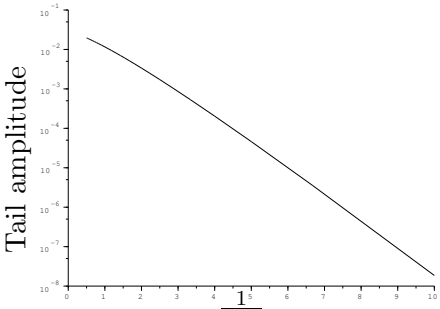

FIGURE 11. Amplitude of the tails of the traveling breather solutions computed numerically in figure 6, expressed as a function of $\frac{1}{p-2}$. The amplitude is computed within the index set S corresponding to $|n - 250| \geq 125$ (i.e. sufficiently far from the breather center). The vertical axis corresponds to $\min_{n\in S} |a_n(0)|$. One has $\max_{n\in S} |a_n(0)| - \min_{n\in S} |a_n(0)| < 3 \cdot 10^{-11}$ for $p \in [2.1, 4]$.

chain of $N = 99$ particles to reduce computation time. Due to the scaling invariance of (4), we further restrict the numerical study to solutions with unit energy.

As previously, we use the Gaussian approximation of section 33.2 to initiate the Gauss-Newton method and proceed by path following. Numerical computations are performed by fixing $R = 1$ and varying q (then $v = 2 \sin q$). Note that $v \to 0$ when $q \to \pi$, hence the integration time in the shooting method diverges in this limit. For each value of q, a solution with unit energy $\mathcal{H} = |a_1 - a_N|^p + \sum_{n=1}^{N-1} |a_{n+1} - a_n|^p$ is obtained by multiplying a numerical solution with energy $\mathcal{H}$ by $R = \mathcal{H}^{-1/p}$. The velocity v of this new solution is then given by (38).

Figure 12 shows typical traveling breather profiles obtained with the above procedure. They correspond to a localized excitation superposed in most cases to an oscillatory tail. Tail size exhibits important variations with respect to v (or equivalently q) during numerical continuation. This is due to the fact that in the limit of an infinite chain, a continuum of solutions can be expected in the neighborhood of a traveling breather for the same value of (v, θ). Indeed, as discussed in section 33.4-3.4.2), we expect that traveling breathers can be superposed on an oscillatory tail with amplitude and wavenumber linked by equation (54), and the tail amplitude provides an additional free parameter.

We have performed an extensive numerical exploration of the profiles of traveling breathers when q varies in the interval $(\frac{\pi}{2}, \pi)$. We have observed a local drop in the tail size close to

$v = 1.05$, where tail size over breather amplitude is close to $1.6 \cdot 10^{-3}$. At this local minimum, the energy density $|a_{n+1}(0) - a_n(0)|^p$ in the tail is extremely small (of the order of 10^{-16}, i.e. machine precision). This value of v corresponds to θ close to 0, i.e. the solution is close to a solitary wave ($\theta \approx 3.4 \cdot 10^{-4}$ and $q \approx 2.33$). This result suggest that strictly localized solitary waves exist in the DpS equation (4) with $p = 2.5$. Another local drop in tail size occurs close to $v = 0.3$, but the phonemenon is less clear. Indeed, in this region where breather velocity v is relatively small, tail size tends to be small for all values of v. This is consistent with the fact that static breathers (case $v = 0$) are strictly localized [34].

5. Discussion

We have derived several amplitude equations to approximate slowly modulated periodic waves in the DpS equation with nonlinearity exponent close to unity. These models provide analytical approximations of traveling breather solutions with superexponential spatial decay (either Gaussian or with compact support). From a numerical point of view, we have computed exact traveling breather solutions for $p \in (2, 4]$ and compared them to the approximate solutions, observing convergence when $p \to 2^+$. Traveling breathers computed numerically are generally superposed on a small nonvanishing oscillatory tail, except in special cases when they are close to strictly localized solitary waves. In the vibroimpact limit when p becomes large, we have obtained an analytical approximation of the solitary wave excited by an initial perturbation applied to the first particle in the chain. Thanks to the available error bounds relating the Dps dynamics to the Newton's cradle (3) [6] and the resonant granular chain (2) for $\omega \approx 0$ [44], our numerical results (supplemented by analytical approximations) imply the existence of long-lived traveling breather solutions in the above models.

A first problem left open in this study concerns the theoretical validation of the multiscale analysis performed for $p \approx 2^+$. In the spirit of classical modulation theory leading to the NLS equation [26], it would be interesting to prove that sufficiently smooth solutions of the logarithmic NLS equation approximate true solutions of DpS on long time intervals when $p \approx 2$. In this context, the log-NLS equation seems more suitable than the fully nonlinear NLS equations (22) or (23), since its well-posedness has been established in [11], and consistency estimates in $\ell_2(\mathbb{Z})$ appear more tractable. However some nontrivial features can be expected due to the non-Lipschitzian character of the leading logarithmic nonlinearity in (13).

Another open problem concerns an existence proof for exact traveling breather solutions of the DpS equation. According to our numerical results, we conjecture the existence of solutions of (4)-(26) (close to the Gaussian or compacton approximations for $p \approx 2$), consisting of strictly localized solitary waves for $\theta = 0\,(2\pi)$, and superposed on nonvanishing oscillatory tails for $\theta \neq 0\,(2\pi)$. These problems might be addressed using critical point theory in the spirit of the works [16, 17] concerning periodic and quasiperiodic traveling waves in generalized DNLS equations. Indeed equation (57) corresponds (for localized solutions) to the Euler equation for the Lagrangian

$$S(y, \bar{y}) = \int_{\mathbb{R}} \frac{i\,v}{2}\,(y\,\bar{y}' - y'\,\bar{y}) + \frac{2}{p}\,|e^{-i\theta}\,y(\xi + 1) - y(\xi)|^p\,d\xi.$$

It is also important to notice that our numerical procedure does not penalize the tail size during minimization, therefore we may have missed strictly localized traveling breathers existing away from $\theta = 0\,(2\pi)$. This problem constitutes an interesting possible extension of the numerical part of this work. Traveling breathers with minimal tail are expected to display negligible dispersion when their tail is truncated in the direction of propagation, whereas dispersion should be much stronger for larger tails. Consequently, solitary waves or traveling breather with minimal tail are good candidates to approximate (dispersive) "attractors" forming after

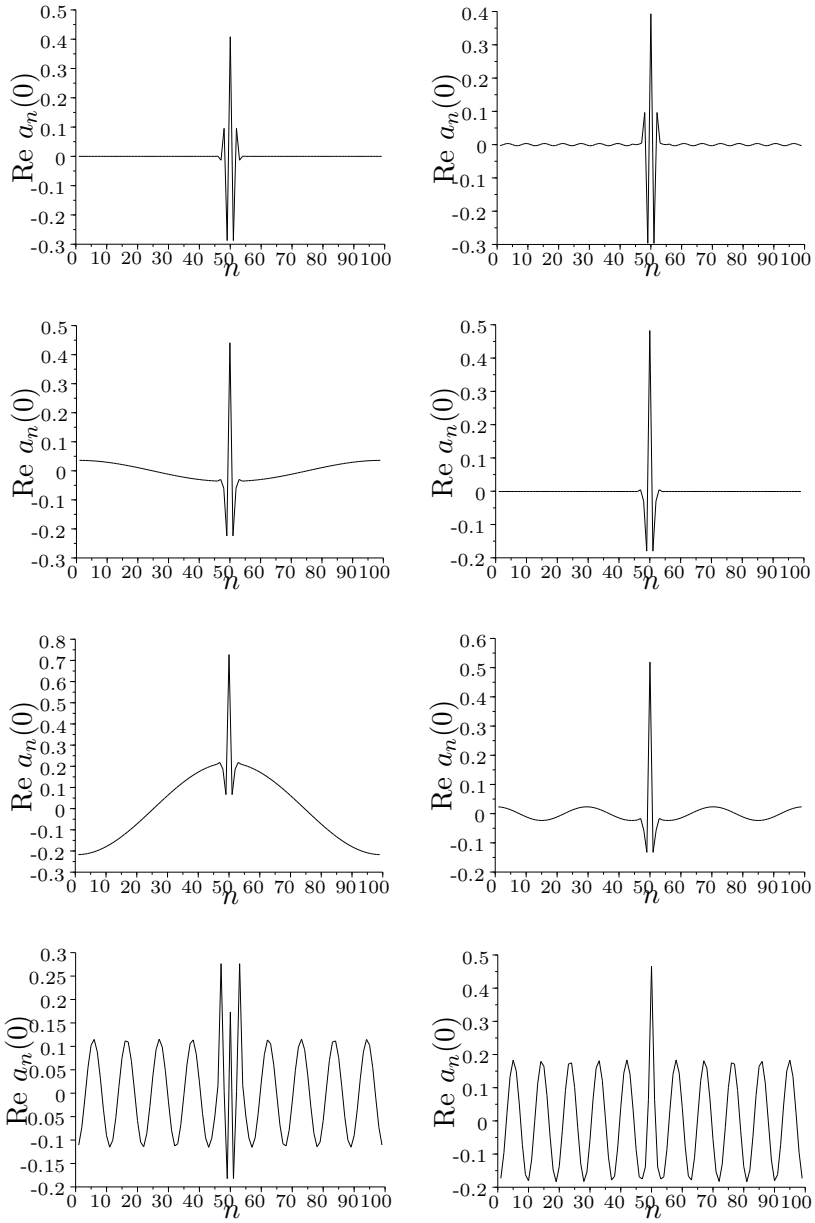

FIGURE 12. Real part of traveling breather solutions with unit energy $\mathcal{H}$, for the following parameter values (from top to bottom and left to right) : $v \approx 0.08$ ($q \approx 3.08$, $\theta \approx -0.92$), $v \approx 0.16$ ($q \approx 3.02$, $\theta \approx -1.42$), $v \approx 1.02$ ($q \approx 2.36$, $\theta \approx -0.06$), $v \approx 1.05$ ($q \approx 2.33$, $\theta \approx 3.4 \cdot 10^{-4}$), $v \approx 1.08$ ($q \approx 2.30$, $\theta \approx 0.06$), $v \approx 1.17$ ($q \approx 2.21$, $\theta \approx 0.21$), $v \approx 1.22$ ($q \approx 1.86$, $\theta \approx 0.52$), $v \approx 1.39$ ($q \approx 1.63$, $\theta \approx 0.57$). Computations are performed for $p = 5/2$.

excitation of a single lattice site, which display a small oscillatory tail at the rear of the pulse and decay to 0 at the front.

Another interesting theoretical problem concerns the analysis of localized waves in the limit $p \to +\infty$. When p is large but finite in (4), it would be interesting to prove the existence of exact solitary waves close to the approximate solutions obtained in the present study, and to

approximate the time-evolution of general classes of initial conditions. Results in this direction have been obtained for some classes of nonlinear wave equations [68] and nonlinear diffusion equations (see [3] and references therein), but to the best of our knowledge there is currently no rigorous theory available for discrete NLS-type systems.

Acknowledgments

The author thanks the PAZI Fund (Israel Atomic Energy Commission) (Grant No. 263/15) for financial support. The author is grateful to Y. Starosvetsky and O. Gendelman for stimulating discussions.

References

[1] E. Afshari and A. Hajimiri. Nonlinear transmission lines for pulse shaping in silicon, *IEEE Journal of Solid-State Circuits 40* (2005), 744-752.
[2] K. Ahnert and A. Pikovsky. Compactons and chaos in strongly nonlinear lattices, *Phys. Rev. E 79* (2009), 026209.
[3] F. Andreu, J.M. Mazón, J.D. Rossi and J. Toledo. The limit as $p \to \infty$ in a nonlocal p-Laplacian evolution equation: a nonlocal approximation of a model for sandpiles, *Calc. Var. 35* (2009), 279-316.
[4] D. Bambusi and A. Ponno. On metastability in FPU, *Comm. Math. Phys. 264* (2006), 539-561.
[5] I. Bialynicki-Birula and J. Mycielski. Nonlinear wave mechanics, *Annals of Physics 100* (1976), 62.
[6] B. Bidégaray-Fesquet, E. Dumas and G. James. From Newton's cradle to the discrete p-Schrödinger equation , *SIAM J. Math. Anal. 45* (2013), 3404-3430.
[7] A. Björck, *Numerical methods for least squares problems*, SIAM, Philadelphia, 1996.
[8] L. Bonanomi, G. Theocharis and C. Daraio. Wave propagation in granular chains with local resonances, *Phys. Rev. E 91* (2015), 033208.
[9] J.P. Boyd and G.-Y. Chen. Weakly nonlinear wavepackets in the Korteweg-de Vries equation: the KdV/NLS connection, *Mathematics and Computers in Simulation 55* (2001), 317-328.
[10] D.K. Campbell et al, editors. The Fermi-Pasta-Ulam problem : the first 50 years, *Chaos 15* (2005).
[11] T. Cazenave and A. Haraux. Equations d'évolution avec non linéarité logarithmique, *Annales Faculté des Sciences Toulouse 2* (1980), 21-51.
[12] A. Chatterjee. Asymptotic solution for solitary waves in a chain of elastic spheres, *Phys. Rev. E 59* (1999), 5912-5919.
[13] Q. Dou, J. Cuevas, J.C. Eilbeck and F.M. Russell. Breathers and kinks in a simulated breather experiment, *Discrete Contin. Dyn. Syst. Ser. S 4* (2011), 1107-1118.
[14] O.A. Dubovsky and A.V. Orlov. Emission of supersonic soliton wave beams - generators of restructuring of nanocrystals under atom bombardment, and the self-organization of a dynamic superlattice of complexes of soliton atomic vibrations, *Phys. of solid state 52* (2010), 899-903.
[15] J.M. English and R.L. Pego. On the solitary wave pulse in a chain of beads, *Proc. Amer. Math. Soc. 133*, n. 6 (2005), 1763-1768.
[16] M. Fečkan and V.M. Rothos. Travelling waves of discrete nonlinear Schrödinger equations with nonlocal interactions, *Applicable Analysis 89* (2010), 1387-1411.
[17] M. Fečkan and V.M. Rothos. Travelling waves of forced discrete nonlinear Schrödinger equations, *Discrete Contin. Dyn. Syst. Ser. S 4* (2011), 1129-1145.
[18] S. Flach. Conditions of the existence of localized excitations in nonlinear discrete systems, *Phys. Rev. E 50* (1994), 3134-3142.
[19] S. Flach. Existence of localized excitations in nonlinear Hamiltonian lattices, *Phys. Rev. E 51* (1995), 1503-1507.
[20] S. Flach and A. Gorbach. Discrete breathers : advances in theory and applications, *Physics Reports 467* (2008), 1-116.
[21] S. Flach and K. Kladko. Moving discrete breathers ?, *Physica D 127* (1999), 61-72.
[22] S. Flach and C.R. Willis. Discrete Breathers, *Physics Reports 295* (1998), 181-264.
[23] G. Friesecke and J.A Wattis. Existence theorem for solitary waves on lattices, *Commun. Math. Phys. 161* (1994), 391-418.
[24] G. Gantzounis, M. Serra-Garcia, K. Homma, J. M. Mendoza and C. Daraio. Granular metamaterials for vibration mitigation, *Journal of Applied Physics 114* (2013), 093514.

[25] O.V. Gendelman and L.I. Manevitch. Discrete breathers in vibroimpact chains: Analytic solutions, *Phys. Rev. E 78* (2008), 026609.
[26] J. Giannoulis and A. Mielke. Dispersive evolution of pulses in oscillator chains with general interaction potentials, *Discr. Cont. Dyn. Syst. B 6* (2006), 493-523.
[27] J. Giannoulis, M. Herrmann and A. Mielke. Lagrangian and Hamiltonian two-scale reduction, *Journal of Mathematical Physics 49* (2008), 103505:1-42.
[28] M. Herrmann. Unimodal wavetrains and solitons in convex Fermi-Pasta-Ulam chains, *Proc. R. Soc. Edinb. Sect. A-Math. 140* (2010), 753-785.
[29] G. Iooss and K. Kirchgässner. Travelling waves in a chain of coupled nonlinear oscillators, *Commun. Math. Phys. 211* (2000), 439-464.
[30] G. Iooss and G. James, Localized waves in nonlinear oscillator chains, *Chaos 15* (2005), 015113.
[31] G. James. Nonlinear waves in Newton's cradle and the discrete p-Schrödinger equation, *Math. Models Meth. Appl. Sci. 21* (2011), 2335-2377.
[32] G. James, P.G. Kevrekidis and J. Cuevas. Breathers in oscillator chains with Hertzian interactions, *Physica D 251* (2013), 39-59.
[33] G. James and Y. Sire. Center manifold theory in the context of infinite one-dimensional lattices, in *The Fermi-Pasta-Ulam Problem. A Status Report*, G. Gallavotti Ed., *Lecture Notes in Physics 728* (2008), p. 207-238.
[34] G. James and Y. Starosvetsky. Breather solutions of the discrete p-Schrödinger equation, in *Localized Excitations in Nonlinear Complex Systems*, Eds. R. Carretero-González, J. Cuevas-Maraver, D. Frantzeskakis, N. Karachalios, P. Kevrekidis, F. Palmero-Acebedo, *Nonlinear Systems and Complexity 7* (2014), 77-115, Springer.
[35] G. James and D. Pelinovsky. Gaussian solitary waves and compactons in Fermi-Pasta-Ulam lattices with Hertzian potentials, *Proc. R. Soc. A. 470* (2165), 2014.
[36] L.A. Kalyakin. Long wave asymptotics. Integrable equations as asymptotic limits of non-linear systems, *Russian Math. Surveys 44* (1989), 3-42.
[37] P.G. Kevrekidis, *The Discrete Nonlinear Schrödinger Equation: Mathematical Analysis, Numerical Computations and Physical Perspectives*, Springer-Verlag, Heidelberg, 2009.
[38] P.G. Kevrekidis, A.G. Stefanov and H. Xu. Traveling Waves for the Mass in Mass Model of Granular Chains, *Letters in Mathematical Physics 106* (2016), 1067-1088.
[39] P. G. Kevrekidis, A. Vainchtein, M. Serra Garcia and C. Daraio. Interaction of traveling waves with mass-with-mass defects within a Hertzian chain, *Phys. Rev. E 87* (2013), 042911.
[40] D. Khatri, D. Ngo and C. Daraio. Highly nonlinear solitary waves in chains of cylindrical particles, *Granular Matter 14* (2012), 63-69.
[41] E. Kim and J. Yang. Wave propagation in single column woodpile phononic crystal: Formation of tunable band gaps, *Journal of the Mechanics and Physics of Solids 71* (2014), 33-45.
[42] E. Kim, F. Li, C. Chong, G. Theocharis, J. Yang and P.G. Kevrekidis. Highly Nonlinear Wave Propagation in Elastic Woodpile Periodic Structures, *Phys. Rev. Lett. 114* (2015), 118002.
[43] Yu. S. Kivshar. Intrinsic localized modes as solitons with a compact support, *Phys. Rev. E 48* (1993), R43-R45.
[44] L. Liu, G. James, P. Kevrekidis and A. Vainchtein. Nonlinear waves in a strongly resonant granular chain, *Nonlinearity 29* (2016), 3496-3527.
[45] R.S. MacKay and S. Aubry. Proof of existence of breathers for time-reversible or Hamiltonian networks of weakly coupled oscillators, *Nonlinearity 7* (1994), 1623-1643.
[46] R.S. MacKay. Solitary waves in a chain of beads under Hertz contact, *Phys. Lett. A 251* (1999), 191-192.
[47] T.R.O. Melvin, A.R. Champneys, P.G. Kevrekidis and J. Cuevas. Radiationless traveling waves in saturable nonlinear Schrödinger lattices, *Phys. Rev. Lett. 97* (2006), 124101.
[48] T.R.O. Melvin, A.R. Champneys, P.G. Kevrekidis and J. Cuevas. Travelling solitary waves in the discrete Schrödinger equation with saturable nonlinearity: Existence, stability and dynamics, *Physica D 237* (2008), 551-567.
[49] V.F. Nesterenko, *Dynamics of heterogeneous materials*, Springer Verlag, 2001.
[50] D. Ngo, S. Griffiths, D. Khatri and C. Daraio. Highly nonlinear solitary waves in chains of hollow spherical particles, *Granular Matter 15* (2013), 149-155.
[51] N.-S. Nguyen and B. Brogliato, *Multiple impacts in dissipative granular chains*, Lecture Notes in Applied and Computational Mechanics 72, Springer, 2014.
[52] O.F. Oxtoby and I.V. Barashenkov. Moving solitons in the discrete nonlinear Schrödinger equation, *Phys. Rev. E 76* (2007), 036603.

[53] M. Peyrard and G. James. Intrinsic localized modes in nonlinear models inspired by DNA, *Nonlinear Theory and its Applications (NOLTA), Vol. 3* (2012), 27-51.
[54] M. Porter, P.G. Kevrekidis and C. Daraio. Granular crystals : Nonlinear dynamics meets materials engineering, *Physics Today 68* (2015), 44.
[55] P. Rosenau. Hamiltonian dynamics of dense chains and lattices: or how to correct the continuum, *Phys. Lett. A 311* (2003), 39-52.
[56] P. Rosenau. Compactification of patterns by a singular convection or stress, *Phys. Rev. Lett. 99* (2007), 234102.
[57] G. Schneider. Bounds for the nonlinear Schrödinger approximation of the Fermi-Pasta-Ulam system, *Appl. Anal. 89* (2010), 1523-1539.
[58] G. Schneider and C.E. Wayne. Counter-propagating waves on fluid surfaces and the continuum limit of the Fermi-Pasta-Ulam model. In B. Fiedler, K. Gröger and J. Sprekels, editors, *International Conference on Differential Equations Appl. 5* (1), 69-82 (1998).
[59] K. Sekimoto. Newton's cradle versus nonbinary collisions, *Phys. Rev. Lett. 104* (2010), 124302.
[60] S. Sen, J. Hong, J. Bang, E. Avalos and R. Doney. Solitary waves in the granular chain, *Physics Reports 462* (2008), 21-66.
[61] A.J. Sievers and J.B. Page. Unusual anharmonic local mode systems. In : G.K. Norton and A.A. Maradudin, editors, *Dynamical Properties of Solids 7*, Ch. 3, North-Holland, Amsterdam (1995).
[62] Y. Sire. Travelling breathers in Klein-Gordon lattices as homoclinic orbits to p-tori, *J. Dyn. Diff. Eqs. 17* (2005), 779-823.
[63] Y. Starosvetsky, M. Arif Hasan, A.F. Vakakis and L.I. Manevitch. Strongly nonlinear beat phenomena and energy exchanges in weakly coupled granular chains on elastic foundations, *SIAM J. Appl. Math. 72* (2012), 337.
[64] Y. Starosvetsky, K.R. Jayaprakash, M.A. Hasan and A.F. Vakakis, *Topics on the nonlinear dynamics and acoustics of ordered granular media*, World Scientific, Singapore, 2017.
[65] A. Stefanov and P.G. Kevrekidis. On the existence of solitary traveling waves for generalized Hertzian chains, *J. Nonlinear Sci. 22* (2012), 327-349.
[66] D. Sun, C. Daraio and S. Sen. Nonlinear repulsive force between two solids with axial symmetry, *Phys. Rev. E 83* (2011), 066605.
[67] D. Sun and S. Sen. Nonlinear grain-grain forces and the width of the solitary wave in granular chains : a numerical study, *Granular Matter 15* (2013), 157-161.
[68] T. Tao, The high exponent limit $p \to \infty$ for the one-dimensional nonlinear wave equation, *Analysis and PDE 2* (2009), 235-259.
[69] K. Vorotnikov, Y. Starosvetsky, G. Theocharis and P.G. Kevrekidis. Wave propagation in a strongly nonlinear locally resonant granular crystal, *Physica D 365* (2018), 27-41.
[70] G.B. Whitham, *Linear and nonlinear waves*, Wiley, New York, 1974.
[71] H. Xu, P.G. Kevrekidis and A. Stefanov. Traveling Waves and their Tails in Locally Resonant Granular Systems, *J. Phys. A: Math. Theor. 48* (2015), 195204.

[1] INRIA Grenoble - Rhône-Alpes, Tripop Team-Project, Inovallée, 655 Avenue de l'Europe, 38334 Saint Ismier Cedex, France. Email : guillaume.james@inria.fr., [2] Univ. Grenoble Alpes, CNRS, Inria, Grenoble INP*, LJK, 38000 Grenoble, France, * Institute of Engineering Univ. Grenoble Alpes